Ultrawide-Band Fiber-Optic Control of a Millimeter-Wave Transmit Beamformer

David A. Tulchinsky and Paul J. Matthews, *Member, IEEE*

***Abstract*—An ultrawide-band fiber-optic true time-delay millimeter-wave array transmitter is fully characterized and demonstrated in this paper. The beamformer is based on dispersive-prism optical-delay lines and exhibits squint-free $\pm 60^{\circ}$ steering in azimuth across the entire Ka-band (26.5–40 GHz). This is believed to be the first fully functioning demonstration of a photonically controlled wide-band millimeter-wave transmitter system.**

***Index Terms*—Array signal processing, millimeter-wave antenna arrays, millimeter-wave radar optical fiber delay lines, optical-fiber dispersion.**

I. Introduction

PHASED-ARRAY antenna systems are increasingly used in a variety of applications due to the many inherent advantages of electronically steered beams over those with mechanical steering. The advantages include reduced size, beam agility, beam shaping, multiple beam formation, increased reliability, graceful degradation, and reduced maintenance costs. However, due to the inherent limitations of traditional all-electronic control over the individual array elements, many of these advantages have not been realized. The inherent complexity in the multiplicity of the microwave phase shifters increases the system cost, with weight and loss being additional drawbacks. Furthermore, when an array is scanned with fixed units of phase by electronic phase shifters, there is a limitation of the system bandwidth since the steering direction of the main beam changes with frequency [1].

High-frequency millimeter-wave radars have many advantages over radars in other portions of the electromagnetic spectrum in that they allow for increased tracking accuracy while not being limited by the reduced apertures available in next-generation designs of miniaturized components. However, due to the current state-of-the-art in broad-band system components at these frequencies (power generation, amplification, and control devices), it has been difficult to make the region of the electromagnetic spectrum above 30 GHz more broadly applicable [2]. Furthermore, the technical difficulties involved with the design of electronic millimeter-wave phase shifters, the basic steering element of phased-array beamformers, has remained a challenging problem. Hence, in the millimeter-wave portion of the spectrum, the Rotman lens has traditionally been used for array beamsteering. With the difficulties involved with the fabrication, waveguide loss, and dispersion of these lenses at millimeter-wave frequencies, this approach has not yet achieved suitable performance over very large bandwidths [3], [4].

Numerous photonic architectures have been investigated to address the above limitations [5]–[7]. One key advantage of photonic control is its ability to provide the wide-band true time-delay (TTD) beamforming necessary for many current and future applications. Although there have been many successful demonstrations of TTD photonic beamforming at lower frequency ranges (L- through Ku-bands), most of the techniques are not amenable to wide-band millimeter-wave applications due to the stringent time-delay resolution (subpicosecond) and amplitude and phase-tracking requirements. For example, switched optical delay lines, which are used in a variety of photonic TTD implementations, would require a path length difference of a few micrometers in order to achieve the subpicosecond resolution (least significant bit) needed at 40 GHz. In general, the few previously demonstrated photonically controlled millimeter-wave array transmitters and receivers have exhibited narrow bandwidths or severely limited operating characteristics due to these difficulties [7]–[9].

Here, we demonstrate what we believe is the first photonic ultrawide-band TTD millimeter-wave array transmitter. The technique is an extension of the previously demonstrated dispersive-prism beamformer [10], further demonstrating the flexibility and utility of this technique. The system's optical components have been tested and are able to optically steer a linear array over an extremely wide frequency range (1–50 GHz). The system's overall bandwidth is limited by the individual antenna array elements and microwave components. As a result, the completed system exhibits $\pm 60^{\circ}$ azimuthal steering with no observable beam squint over the entire Ka-band (26.5–40 GHz).

II. System Configuration

A schematic of the transmit array beamforming system is shown in Fig. 1. The main beamformer is based on the fiber-optic dispersive prism approach and provides a wavelength-dependent time delay at each array element, proportional to the position of the corresponding element in the array. This is accomplished via an optical-dispersion gradient in the beamformer. Hence, by tuning the wavelength of the laser, the dispersion gradient is translated into a time-delay gradient at the antenna element output, producing a time-steered far-field pattern.

An external-cavity single-mode semiconductor laser, which is tunable across a wavelength range of 1470–1590 nm, serves

Manuscript received August 31, 2000. This work was supported by the Office of Naval Research.

The authors are with Code 5651, Optical Sciences Division, U.S. Naval Research Laboratory, Washington, DC 20375 USA.

Publisher Item Identifier S 0018-9480(01)05052-9.

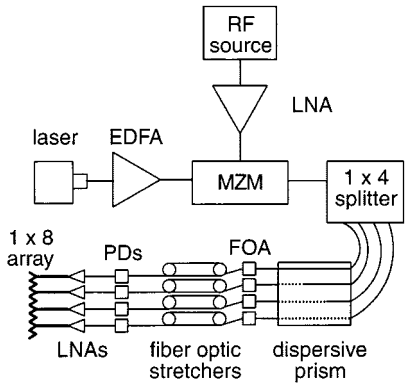

Fig. 1. Schematic diagram of the fiber-optic beamformer.

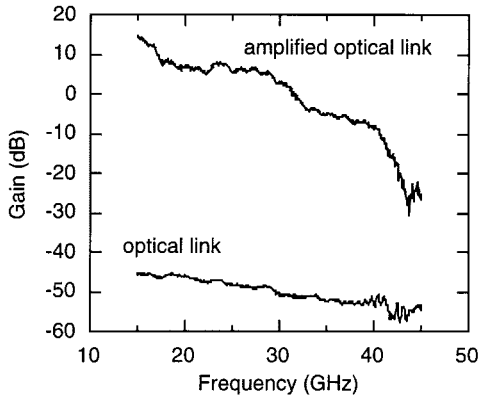

Fig. 2. Frequency response of one of the links in the optical beamformer with and with out the RF pre- and post-amplifiers.

as the optical source for the system. The 1.5-mW output of the laser is amplified to 75 mW by an erbium-doped fiber amplifier (EDFA) and is subsequently modulated by a commercially available Mach–Zehnder modulator (MZM) capable of intensity modulation upwards of 40 GHz. A 0.05–50-GHz preamplifier, with a nominal gain of 30 dB and a saturated output power of 10 mW, is used at the RF input of the MZM to ensure adequate dynamic range at the MZM and to overcome the inherently high RF loss in the microwave cables feeding the system.

The modulated optical carrier is then split and fed into the four-channel fiber-optic dispersive prism. The nominal unit length of high-dispersion (HD) fiber ($D \sim -93.5$ ps/nm $\cdot$ km) in the prism is 25 m. Thus, the four links have 0, 25, 50, and 75 m of HD fiber, respectively. The total length of HD fiber in each link of the prism is known to within ± 2 cm. The overall link lengths are equalized with dispersion-shifted (DS) fiber such that the total difference in the optical time delay between any two links, at the center wavelength (1555 nm), is less than ± 2 ps. Final time trimming is accomplished by adjustment of the fiber-optic stretcher present in each link. The stretchers have a resolution better than 0.25 ps (3.6° at 40 GHz) and exhibit no microwave phase dispersion across the frequency band. Each fiber-optic link also includes a fiber-optic attenuator (FOA) for microwave-frequency independent amplitude matching.

The optical signal is then demodulated by a commercially available 50-GHz p-i-n photodiode (PD). The nonterminated microwave output of the PD is passed through a 6-dB attenuator and then a 60-GHz bias tee, which reduce microwave back-reflections while allowing for voltage biasing of the PDs. The signal is then amplified by broad-band 10–40-GHz low-noise amplifiers (LNAs) having nominal gains of $\sim$35 dB, at the low end of the frequency range. The outputs of the four LNAs are connected to every other element of a 1×8 waveguide antenna array. The array is fabricated from thinned WR-28 waveguide (applicable for Ka-band) with a 4.24-mm element spacing. The unused elements are terminated to reduce unwanted coupling effects between elements. Total radiated output power for the system was less than 10 mW.

III. Laboratory Characterization

After assembly and packaging, the fiber-optic beamforming system was calibrated and tested in the laboratory with a millimeter-wave network analyzer, prior to testing in an anechoic chamber. Several parameters were tested to determine if the system met the design specifications. The fiber-optic HD prism was verified to have a uniform wavelength dispersion, and after final time trimming, the measured maximum time delay error among the channels was ± 0.02 ps, over the full ± 10-nm wavelength tuning range. This extremely small timing/phasing error illustrates the utility of this photonic architecture for millimeter-wave applications.

Fig. 2 shows the typical overall system frequency response of one arm of the fiber-optic beamformer across the 15–45-GHz test band, with 1.0 mA of PD current, showing the response from just the optical link and the optical link with the RF amplifiers. The optical link has an insertion loss of $\sim$45 dB at 15 GHz with an additional 10-dB dropoff by 40 GHz. These are typical parameters for the commercial modulator used ($V_\pi \approx 14.1$ V at 15 GHz and 35.5 V at 40 GHz). The beamformer shows a single-channel insertion gain/loss of $\sim +15$ dB at 15 GHz dropping to -20 dB by 40 GHz. This dropoff in gain is typical for the combination of the MZM with the LNA used for postamplification.

An important parameter for an ultrawide-band array system is the amplitude and phase tracking of the individual link responses across the full instantaneous bandwidth. Fig. 3(a) and (b) shows the amplitude and phase tracking of all four links without the LNA amplifiers in place, respectively. Fig. 3(c) and (d) shows the corresponding responses with the insertion of the LNA postamplifiers. In both figures, the zero dispersion link is taken as the reference by calibrating the network analyzer on its response. Without the LNAs, we observe good amplitude tracking with a rms deviation of $\sim \pm 0.5$ dB across the measured frequency range with the exception of the most dispersive link. This link used a PD from a different production run from the others. When this diode is included, the deviation rises to $\sim \pm 1.1$-dB rms. The unamplified phase tracking has a deviation of $\sim \pm 4.6°$ rms. With the LNAs in place, the system amplitude tracking deviation increases to $\sim$1.8-dB rms, while the phase tracking deviation rises to $\sim$8.0° rms. The overall system gain and dynamic range are limited by the low optical power that is available at the photodetectors and the unavailability of a more efficient MZM in the frequency range of interest.

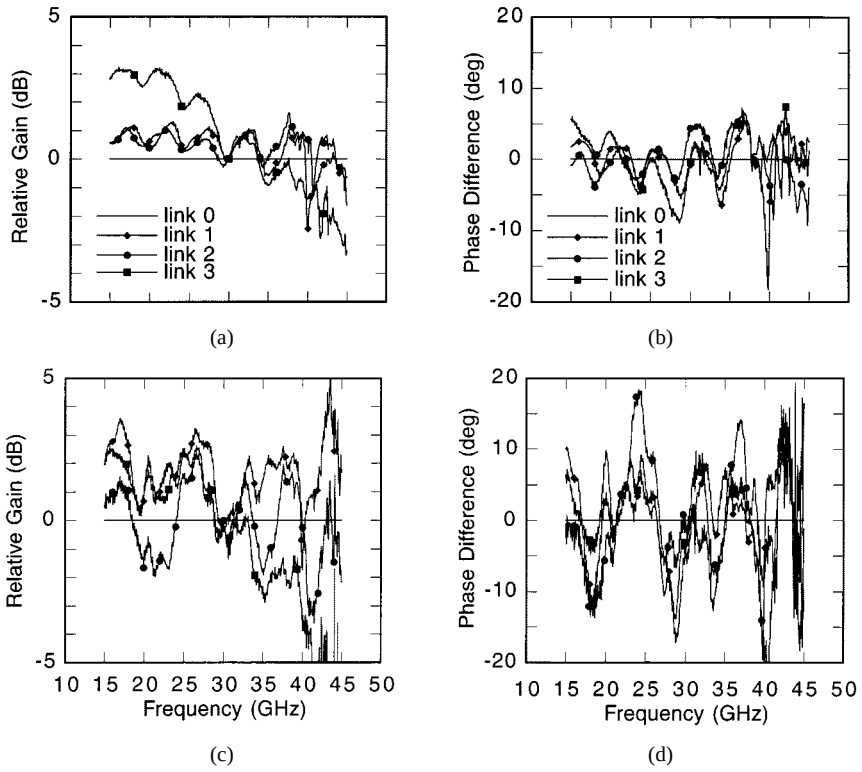

Fig. 3. (a) Amplitude and (b) phase tracking response among the four links without the final low-noise RF amplifiers. (c) Amplitude and (d) phase tracking response between the four links with the final low-noise RF amplifiers. In all plots, the number zero link is the reference.

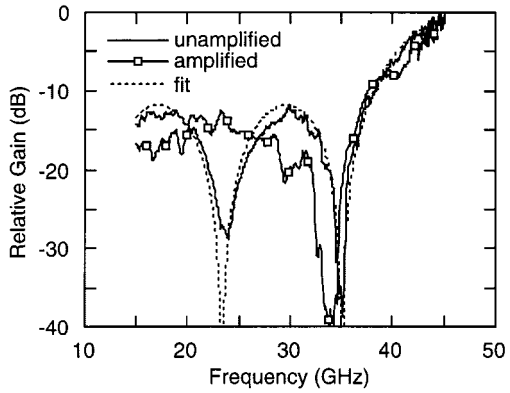

Fig. 4. Laboratory characterization of the broadside (0°) frequency response of the fiber-optic beamformer with laser adjusted for optical steering to 45° azimuth ($\lambda = 1564.2$ nm). The beamformer with and without the final low-noise RF amplifiers, as well as a calculated pattern are shown.

Injecting the microwave outputs of each optical link into a microwave four-way combiner allows for the testing of the systems ability to steer in one dimension in the laboratory. By summing the beamformer's outputs in this manner, a network analyzer can be used to measure the expected radar range broadside (0°) antenna intensity verses frequency response. With the beamformer steered to $+45°$, Fig. 4 shows the measured broadside response for the array with and without the LNAs in place. The theoretical four-element pattern is also shown for comparison. Without the LNAs in place, the performance of the system closely matches the theoretical predictions. Upon insertion of the LNAs, the near doubling of the amplitude and phase mismatch degrades the array pattern to the point where the null at 23.5 GHz is not evident and the position of the 35.0-GHz null has been shifted by 1 GHz. Despite these problems, the position of the main lobe indicates that the amplified system does steer the main beam to the correct angle.

To obtain a better understanding of how the amplitude and phase errors effect the overall system response, calculations of the response of a four-element beamformer were conducted with random errors added to each element, individually in both phase and amplitude. Fig. 5 illustrates how these errors degrade the broadside antenna response. Fig. 5(a) shows the expected response of an antenna steered to 45° and measured at broadside with no signal errors. Fig. 5(b) and (c) adds 3° random error into the phase and 25% random error into the amplitude, respectively. Each of these errors degrades the antenna pattern, and limits the null depth to ∼10 dB below the sidelobe level. The errors tend to deform the shapes of the sidelobes and broaden the nulls. When error in both phase and amplitude are introduced, as is shown in Fig. 5(d), the beam nulls degrade to ∼5 dB below the sidelobes. Despite errors of this size, the position and magnitude of the main beam remains largely unaffected. While these calculations are not a true reflection of the actual mismatch among the beamforming elements, they do suggest that at these levels, errors in amplitude and phase can significantly degrade system performance.

IV. Range Results

The antenna array and fiber-optic beamformer were then tested in a compact anechoic millimeter-wave radar range. A network analyzer was used to drive the RF input of the

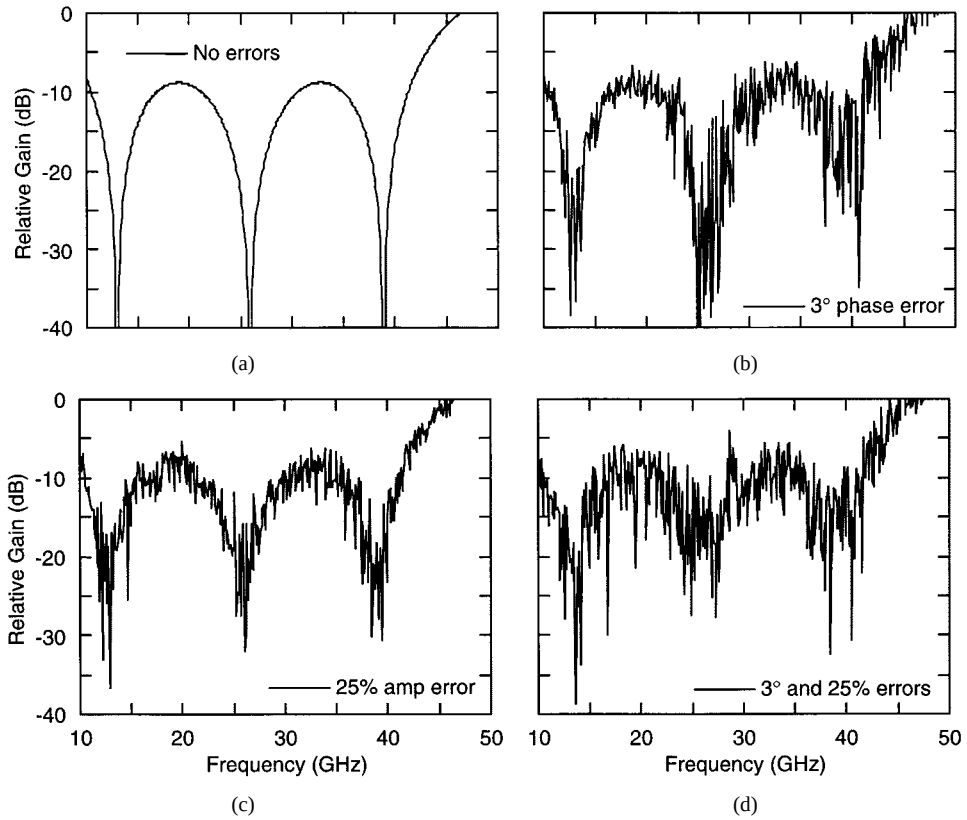

Fig. 5. Calculations of the laboratory patterns measured in Fig. 4 with: (a) no noise, (b) 3° of phase noise, (c) 25% amplitude noise, and (d) 3° phase noise and 25% amplitude noise added to each arm of the beamformer in the calculation.

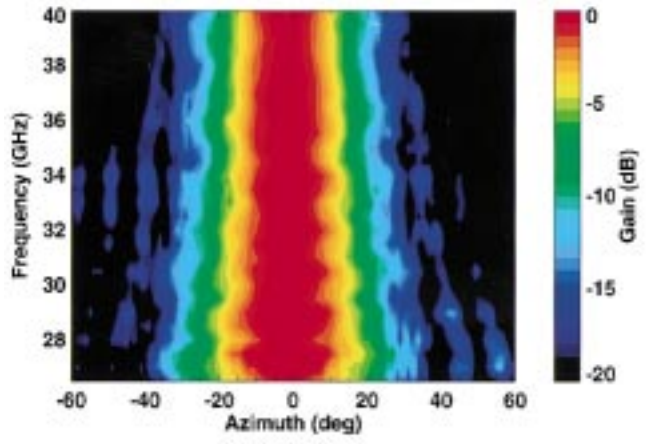

Fig. 6. Transmitted intensity plot as a function of mechanical angle and frequency for a single element of the 1×8 waveguide antenna array steered for broadside radiation (0°). The image is normalized for the frequency response of the system.

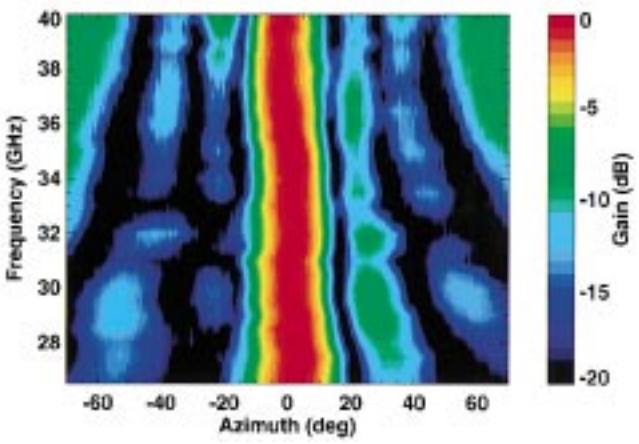

Fig. 7. Array pattern intensity plot as a function of mechanical angle and frequency with the laser adjusted for broadside radiation ($\lambda = 1555.0$ nm). The image is normalized for the frequency response of the system.

system. The radiation from the transmit array was focused onto the receive antenna by an off-axis parabolic microwave mirror. Azimuthal scans were taken across a $\pm 70^{\circ}$ range in 0.25° increments, at frequencies ranging from 20 to 45 GHz in 0.5-GHz increments. The frequency scans were limited on the low-frequency end by the cutoff frequency of the WR-28 waveguide ($f_c \approx 21$ GHz) and on the high-frequency end by the rolloff ($\sim$40 GHz) of the millimeter-wave postamplifiers.

Fig. 6 shows a single-element intensity pattern across the Ka-band (26.5–40 GHz) for a radiating aperture made from a piece of RG-28 thinned waveguide. The element pattern gives an indication of how well the array may be expected to perform over a broad range of steering angles and frequencies. This image, as well as the images in Figs. 7 and 8(a), have been normalized for the frequency response of the system. This single-element pattern does not include any mutual coupling effects, which also can affect the actual array performance.

A measured broadside intensity plot of the transmitted antenna pattern across the Ka-band is shown in Fig. 7 as a function of azimuth and frequency. This image has not been nor-

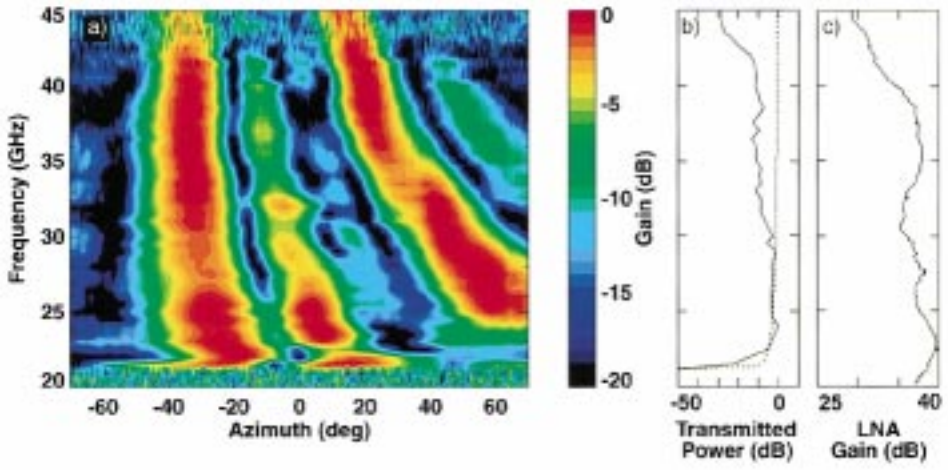

Fig. 8. (a) Array pattern intensity plot as a function of mechanical angle and frequency with the laser adjusted for optical steering to -30° azimuth ($\lambda = 1561.5$ nm). The image is normalized for the frequency response of the system. (b) Intensity as a function of frequency for the measured array pattern in (a) at -30° steering (solid) and the calculated response for WR-28 waveguide (dashed). (c) Measured gain as a function of frequency for one of the low noise postamplifiers used in this system.

malized for the antenna element pattern of the array. The laser was tuned to 1555.0 nm to produce the expected broadside (0°) steering angle. The main lobe is readily discernible at the expected steered angle and exhibits squint free operation over the full 26.5–40-GHz frequency range. The first grating lobe, calculated to be $\sim \pm 60^{\circ}$ away from the main beam at 40 GHz is clearly visible. The two expected sidelobes are also visible on either side of the main beam.

An example of the ultrawide-band frequency capability of this system is demonstrated by the transmitted intensity antenna pattern shown in Fig. 8(a) of a beam-steered 30° off of broadside. Again, this image has not been normalized for the antenna element pattern of the array. The laser was tuned to 1561.5 nm to produce the required TTD gradient at the antenna array. The main lobe exhibits squint-free steering over a greater frequency range than is encompassed by the Ka-band. The transmitted frequency is limited on the low-frequency end by the TE_{10} cutoff frequency of the RG-28 waveguide antenna array, which occurs at 21.1 GHz. The anomalies in the steering near the cutoff frequency of the waveguide are due to the nonideal nature of the phase velocity of the electromagnetic waves in the cutoff regime [11]. Fig. 8(b) shows a line scan of Fig. 8(a) taken at the -30° steering angle, depicting the power transmitted as a function of frequency. The calculated rise in transmitted power as a function of frequency for WR-28 waveguide is also shown. On the low-frequency end, the system intensity output matches that of the ideal waveguide near the cutoff. The high-frequency dropoff in transmitted power is an indication of the dropoff in gain of the LNAs above 40 GHz, as is shown in Fig. 8(c), as well as the inefficiencies of the MZM and PDs.

Fig. 9 shows line scans of the relative radiated power as a function of angle for the steered angles of Fig. 9(a) -30°, Fig. 9(b) 0°, Fig. 9(c), and $+45^{\circ}$ at several frequencies spanning the Ka-band, demonstrating squint-free steering. It is clear that the system is able to operate squint free across the entire Ka-band, with an equally wide instantaneous bandwidth. The bandwidth of the system being solely limited by the microwave components in the system.

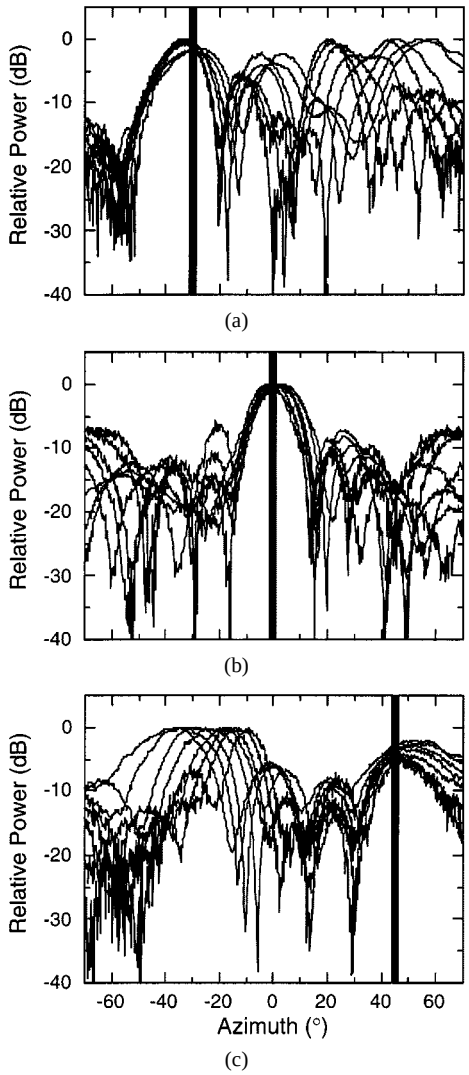

Fig. 9. Relative radiated power as a function of mechanical angle for optical steering to (a) -30°, (b) 0°, and (c) $+45^{\circ}$ in azimuth at frequencies (26.5, 28, 30, 32, 34, 36, 38, 40 GHz) across the Ka-band. The power is normalized to the peak of each curve. The black vertical line is a guide to the eye to indicate where the beam is steered. The data in (a) and (b) are from line scans of Fig. 8(a) and Fig. 7, respectively.

V. Conclusions

We have developed and demonstrated an ultrawide-band transmit beamformer for millimeter-wave transmit arrays. The system is based on the fiber-optic dispersive prism architecture using only commercially available components. The beamformer was characterized for microwave frequency response, dynamic range, and amplitude and phase-tracking errors. Additionally, it was used to drive every other element of a 1×8 waveguide array, and steered antenna patterns were measured in an anechoic chamber. The system demonstrated squint-free array steering across a $\pm 60^{\circ}$ azimuthal span and over the entire Ka-band (26.5–40 GHz). We believe this to be the first demonstration of an ultrawide-band TTD photonically steered millimeter-wave transmit array.

References

[1] R. C. Hansen, *Phased Array Antennas*. New York: Wiley, 1998.

[2] W. C. Pittman, "Introductory Remarks: Forward," presented at the Millimeter-Wave Power Generation Beam Contr. Workshop, 1993.

[3] Y. M. Tao and G. Y. Delise, "Lens-fed multiple beam array for millimeter wave indoor communications," presented at the 1997 IEEE AP-S Int. Symp.

[4] E. O. Raush, A. F. Peterson, and W. Wiebach, "Electronically scanned millimeter wave antenna using a Rotman lens," presented at the RADAR '97 Conf.

[5] H. Zmuda and E. N. Toughlian, *Photonic Aspects of Modern Radar*. Norwood, MA: Artech House, 1994.

[6] N. A. Riza, *Selected Papers on Photonic Control Systems for Phased Array Antennas*, ser. SPIE Milestone. Philadelphia, PA: SPIE, 1997, vol. MS 136.

[7] G. W. Webb, S. C. Rose, M. S. Sanchez, and J. M. Osterwalder, "Experiments on an optically controlled 2-D scanning antenna," presented at the 1998 Antenna Applicat. Symp., Monticello, IL.

[8] L. L. S. Huang, C. H. Lee, and H. L. A. Hung, "Optically controlled generation and true-time-delay phase shifts of broad-band 60-GHz signals," *IEEE Microwave Guided Wave Lett.*, vol. 45, pp. 42–44, Feb. 1993.

[9] V. A. Manasson, L. S. Sadovnik, and V. A. Yepishin, "An optically controlled MMW beam-steering antenna based on a novel architecture," *IEEE Trans. Microwave Theory Tech.*, vol. 45, pp. 1497–1500, Aug. 1997.

[10] R. D. Esman, M. Y. Frankel, J. L. Dexter, L. Goldberg, M. G. Parent, D. Stilwell, and D. G. Cooper, "Fiber-optic prism true time-delay antenna feed," *IEEE Photon. Technol. Lett.*, vol. 5, pp. 1347–1349, Nov. 1993.

[11] S. Ramo, J. R. Whinnery, and T. V. Duzer, *Fields and Waves in Communications Electronics*, 3rd ed. New York: Wiley, 1994, pp. 417–428.

David A. Tulchinsky, photograph and biography not available at time of publication.

Paul J. Matthews (M'99), photograph and biography not available at time of publication.